



Surface-directed spinodal decomposition in hafnium silicate thin films

J. Liu,¹ X. Wu,² W. N. Lennard,¹ and D. Landheer²

¹*Department of Physics and Astronomy, University of Western Ontario, London, Ontario, Canada N6A 3K7*

²*Institute for Microstructural Sciences, National Research Council of Canada, Ottawa, Ontario, Canada K1A 0R6*

(Received 13 April 2009; revised manuscript received 9 June 2009; published 16 July 2009)

Hf distributions in as-grown and annealed $(\text{HfO}_2)_{0.25}(\text{SiO}_2)_{0.75}$ films with thicknesses in the range of 4–19 nm were investigated by high-resolution transmission electron microscopy, high angle annular dark field scanning transmission electron microscopy and angle-resolved x-ray photoelectron spectroscopy. Composition waves normal to the film surface were observed providing evidence for surface-directed spinodal decomposition in the pseudobinary $(\text{HfO}_2)_x(\text{SiO}_2)_{1-x}$ alloy system.

DOI: [10.1103/PhysRevB.80.041403](https://doi.org/10.1103/PhysRevB.80.041403)

PACS number(s): 68.37.Og, 64.75.St, 05.70.Fh

Spinodal decomposition (SD) is a diffusional phase separation whereby a local composition fluctuation reduces the overall free energy of the system.¹ In the bulk of a binary mixture experiencing SD, a description of the composition in the solution will be a superposition of sine waves of fixed wavelength, but random in orientation, phase, and amplitude in the initial stage where the linear theory is applicable.² The average size of the single-phase domains then grows with time corresponding to a coarsening of the structure.³ Recently, it has been recognized that for thin-film geometry, SD may interact with wetting phenomena resulting in a very different structure at the surfaces compared to the bulk behavior.^{4–7} This phenomenon has been called surface-directed spinodal decomposition (SDSD). SDSD simulations show that a composition wave perpendicular to the surface forms at the surface due to the preferential attraction of the surface to one of the two components.⁶ This wave then propagates into the bulk of the film and decays because of thermal noise. Most experimental studies in SDSD have been carried out in polymer mixtures where a small self-diffusion coefficient slows the SD dynamics and the associated phase diagrams can be tailored.^{4,5} While it is predicted that SD could occur generally in any two-component system whose phase diagram shows a miscibility gap, such as ZrO_2 - SiO_2 , HfO_2 - SiO_2 , La_2O_3 - SiO_2 , Y_2O_3 - SiO_2 ,⁸ and Al_2O_3 - SiO_2 , experimental observations of SDSD in thin solid films have never been reported.

As complementary metal oxide semiconductor (CMOS) technology progresses, scaling of the traditional gate dielectrics, i.e., SiO_2 and SiO_xN_y , enters the nanometer regime.⁹ In this thickness range, the increase in direct tunneling current through the gate oxide raises power consumption and device reliability issues. Numerous efforts have been carried out to search for materials (so called high κ) with dielectric constants larger than SiO_2 so that a thick gate insulator layer could be used to reduce the leakage current while improving transistor performance.¹⁰ Pseudobinary alloys $(\text{ZrO}_2)_x(\text{SiO}_2)_{1-x}$ and especially $(\text{HfO}_2)_x(\text{SiO}_2)_{1-x}$ are of great interest as replacement high- κ dielectric materials for SiO_2 and SiO_xN_y in CMOS technology.¹¹ Amorphous thin films are suitable for CMOS transistors since grain boundaries in polycrystalline structures can become conducting paths.¹² However, phase separation has been reported in $(\text{ZrO}_2)_x(\text{SiO}_2)_{1-x}$ and $(\text{HfO}_2)_x(\text{SiO}_2)_{1-x}$ systems

with $x=0.15$ – 0.80 at a typical dopant activation temperature with the attendant crystallization of ZrO_2 or HfO_2 .^{13,14} Kim and McIntyre⁸ calculated the metastable extensions of the miscibility gap and spinodal for the ZrO_2 - SiO_2 system based on available phase diagrams and predicted that, upon rapid thermal annealing at conventional device processing temperatures, the $(\text{ZrO}_2)_x(\text{SiO}_2)_{1-x}$ system with composition in the spinodal ($x=0.1$ – 0.6) will phase separate into two phases having compositions given by the metastable extensions of the miscibility gap. They further simulated the effect of the $(\text{ZrO}_2)_x(\text{SiO}_2)_{1-x}$ film/Si substrate interface on SD and predicted a composition wave normal to the substrate surface, which decays when propagating into the bulk of the film. It is expected that the $(\text{HfO}_2)_x(\text{SiO}_2)_{1-x}$ system would experience the same kind of phase separation during annealing due to the similarity of the chemical properties of the Hf and Zr silicates. However, such a SDSD in oxide systems has never been observed experimentally. In this Rapid Communication, we report the first observation of SDSD in thin solid films, i.e., $(\text{HfO}_2)_x(\text{SiO}_2)_{1-x}$ films, with $x \approx 0.25$, which is in the predicted spinodal range of the $\text{Zr}(\text{Hf})\text{O}_2$ - SiO_2 system.

Thin films with composition $(\text{HfO}_2)_{0.25}(\text{SiO}_2)_{0.75}$ were grown on *p*-type Si (100) substrates by atomic layer deposition (ALD) using the precursors tetrakis(diethylamido)hafnium and tris(2-methyl-2-butoxy)silanol. The detailed growth procedure has been described previously.¹⁵ ALD utilizes the self-limiting reaction mechanism between gaseous precursors and the surface species to produce a thin-film one atomic layer at a time.¹⁶ During a growth cycle, each precursor was introduced separately into the deposition chamber. Alternate precursor pulses were separated by an inert gas purge step. The precursor pulse cycles were repeated until the desired film thickness was achieved. Prior to deposition, the substrate was heated to 500 °C for 300 s in O_2 environment to oxidize the H-terminated surface. *In situ* x-ray photoelectron spectroscopy (XPS) data showed that the oxidation process resulted in a <0.5 nm Si thermal oxide. Films with thickness in the range of 4–19 nm were grown while the substrates were held at 350 °C. In order to investigate the Hf depth profiles in both the as-grown and annealed films, $\langle 011 \rangle$ cross-sectional transmission electron microscope (TEM) samples were prepared using standard dimpling and ion milling procedures and characterized by high-resolution transmission electron microscopy (HRTEM) and high angle an-

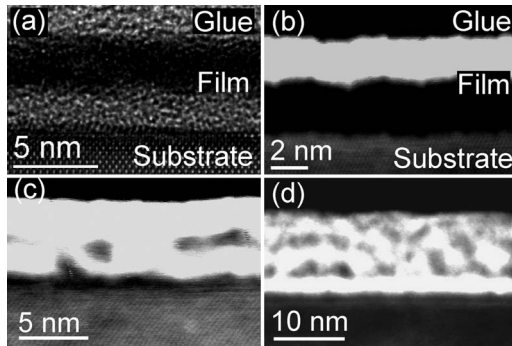


FIG. 1. (a) BF and (b) DF image of a 5 nm as-grown film. DF images of (c) 6.4 and (d) 12 nm as-grown films.

nular dark field scanning transmission electron microscopy (HAADF-STEM) in a JEOL JEM-2100F TEM operating at 200 kV. The HRTEM and HAADF-STEM images are referred to as bright field (BF) and dark field (DF) images, respectively. Film compositions near the surface were also investigated by angle-resolved XPS (ARXPS) using monochromatic Al $K\alpha$ x rays. An *ex situ* rapid thermal anneal (RTA) was subsequently performed in N_2 at 800 °C for 6 s.

Figures 1(a) and 1(b) show the BF and DF images of a 5 nm as-grown film. In Fig. 1(a), the darker area near the surface indicates a region of higher Hf concentration relative to the brighter area close to the substrate. The contrast in Fig. 1(b) is reversed relative to Fig. 1(a) such that the DF image is more sensitive to the atomic number of the constituent atoms. Both images confirm the Hf-rich top region and the Hf-deficient (i.e., Si-rich) bottom region of the film. Additional TEM images of thinner (~ 4 nm) as-grown films show a similar structure. Figures 1(c) and 1(d) show the DF images of 6.4 and 12 nm films, respectively. In both films, there are Hf-deficient layers at the substrate interface of thickness 0.6 and 1 nm, respectively. These data show that during the film deposition process when the film thickness increases from 5 to >6 nm, some Hf atoms in the Hf-rich layer apparent in Fig. 1(b) diffuse toward the substrate. It is difficult to determine whether the entire Hf-deficient layer adjacent to the substrate [see Fig. 1(c)] is thermal SiO_2 formed initially during the substrate oxidation process. The Hf-deficient layer in Fig. 1(b) is not all thermal SiO_2 since its thickness is too large, i.e., significantly >0.5 nm, and it is therefore a Si-rich layer of the film.

Figure 2(a) shows the BF image of the 5 nm film [Figs. 1(a) and 1(b)] after RTA. Figures 2(b) and 2(d) are the DF images of the films shown in Figs. 1(c) and 1(d), respectively, after RTA. The thickness of all films decreases slightly due to densification during annealing. The Hf profile for the 5 nm film is little changed following RTA: the film separates into two layers with the layer closer to the substrate still Si rich. The 6.4 nm film separates into three layers: a Si-rich layer sandwiched between two Hf-rich layers. The 0.5 nm interface layer in Fig. 2(b) is Si thermal oxide formed during the substrate oxidation process. An 8 nm film after RTA [Fig. 2(c)] consists of four layers starting from the bottom (i.e., substrate): Si-rich, Hf-rich, Si-rich, and Hf-rich. Figure 2(d) shows a very thin ~ 1 nm Si-rich layer on the substrate with

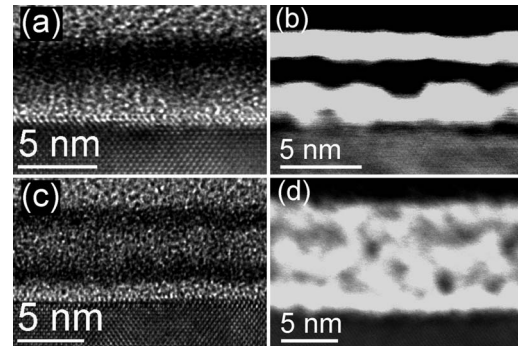


FIG. 2. (a) BF image of film shown in Fig. 1(a) after RTA; (b) DF image of film shown in Fig. 1(c) after RTA; (c) BF image of an 8 nm film after RTA; and (d) DF image of film shown in Fig. 1(d) after RTA.

a ~ 2 nm Hf-rich layer on top similar to Fig. 1(d). Above these two layers, Hf-rich clusters are mixed with Si-rich clusters.

The layered structure shown in the above TEM images provides evidence that SDSD occurs in $(HfO_2)_{0.25}(SiO_2)_{0.75}$ films. A composition wave normal to the substrate surface is observed in post-RTA films thinner than 8 nm. If the composition wavelength, λ_C , is defined as the distance between the centers of the two successive Hf-rich layers, then λ_C measured from TEM images [Figs. 2(b) and 2(c)] is ~ 4 nm. If the film is thinner than 8 nm (i.e., $2\lambda_C$), a layered structure is observed via TEM throughout the entire film: the surface layer is Hf rich and the layer closest to the interface can be Si rich or Hf rich depending on the film thickness. If the film thickness is λ_C or $2\lambda_C$, the layer closest to the interface is Si rich. If the film thickness is $1.5\lambda_C$, the layer closest to the interface is Hf rich—a surprising result. The film phase closest to the interface was expected to be Si rich since the $(HfO_2)_{0.25}(SiO_2)_{0.75}$ films were grown on a very thin Si thermal oxide and the Si-rich phase in the films should have a lower interface energy with this oxide layer. As the film thickens to $>2\lambda_C$, a Si-rich layer followed by a Hf-rich layer is observed at the film/Si interface and there is no continuous Hf-rich layer in the center of the film, indicating a tendency for decay of the composition wave.

Figure 3 shows the BF and DF images of a 19 nm as-grown film where HfO_2 crystallites with dimension of 5–8 nm are seen in Fig. 3(a). This observation implies that the nucleation and growth of crystalline HfO_2 have followed SD during the film deposition process. The DF image [Fig. 3(b)] shows that in the 19 nm film, a Si-rich layer is formed on the substrate with a Hf-rich layer above; on top of these two

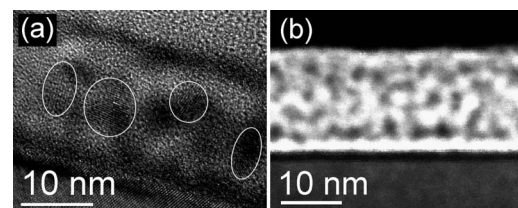


FIG. 3. (a) BF and (b) DF images of a 19 nm as-grown film. Crystalline HfO_2 regions are encircled.

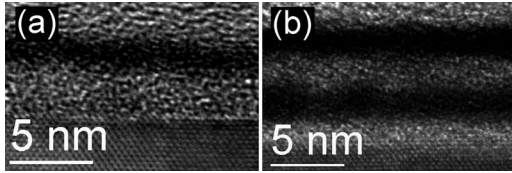


FIG. 4. BF images of (a) 6.4 and (b) 12 nm films after RTA, HF etch, and RTA.

layers, Hf-rich and Si-rich clusters are randomly mixed. This image is similar to the simulation results⁶ for the cross-sectional images of a film experiencing SDSD.

To further study the effect of film thickness on film structure, dilute HF (0.4%) was used to etch back the 6.4 and 12 nm films. Before etching, the $(\text{HfO}_2)_{0.25}(\text{SiO}_2)_{0.75}$ films were subjected to the usual RTA process to reduce the etching rate¹⁷ and to achieve the layered structure shown in Fig. 2(b) for the 6.4 nm film. After etching, the RTA step was repeated. Spectroscopic ellipsometry was used to monitor the etching rate, (i.e., the film thickness was measured after every 4 s etch). For 6.4 nm film, XPS was also used to measure film thickness¹⁸ before and after etching. Figure 4(a) shows the BF image of the 6.4 nm film after RTA, HF etch, and RTA. A 2 nm layer of the film was removed after HF etching; i.e., the top Hf-rich layer in Fig. 2(b) was removed. The Hf-rich layer closest to the substrate in Fig. 2(b) has diffused to the top of the film after the HF etch and following the second RTA, resulting in a structure similar to that in Fig. 2(a), which corresponds to a 5 nm film (annealed) on a Si substrate. The thickness of the film shown in Fig. 4(a) is 1 nm greater than expected after HF etching and RTA, which can likely be explained by oxidation of the Si substrate during the annealing process via water molecules absorbed in the film during the HF etching process. Figure 4(b) shows the BF image of the 12 nm film [Fig. 1(d)] after RTA, HF etch (removing ~ 6 nm), and RTA. The Si-rich layer closest to the substrate is thermal SiO_2 formed after HF etching and the second RTA. The predominantly layered structure, which was not observed for the 12 nm film [see Fig. 2(d)], appears when the film thickness is reduced to a value in the region $\lesssim 2\lambda_C$.

In SDSD, λ_C will increase as the annealing time increases corresponding to a coarsening of the phase separated structures.^{6,8} In order to search for this phenomenon in Hf silicate films, longer time anneals were performed for the 6.4 and 12 nm films. Figures 5(a) and 5(b) show the DF and BF images of the 6.4 and 12 nm films, respectively, after a 600 s anneal in N_2 at 800 °C. Figure 5(a) shows only one Hf-rich

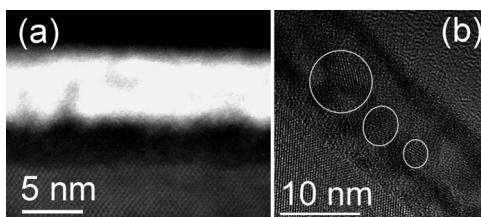


FIG. 5. (a) DF image of 6.4 nm and (b) BF image of 12 nm films, after 600 s anneal. Crystalline HfO_2 regions are encircled.

TABLE I. Hf concentration extracted from ARXPS. θ is the photoelectron takeoff angle.

Film thickness (nm)	Film description	Hf/(Hf+Si)		
		θ (deg)		
		75	45	10
5	As-grown	0.262	0.261	0.249
5	RTA	0.260	0.249	0.225
6.4	As-grown	0.242	0.246	0.228
6.4	RTA	0.225	0.236	0.198
6.4	600 s anneal	0.220	0.223	0.189
12	600 s anneal	0.239	0.235	0.178
12	RTA, HF etch, RTA	0.222	0.212	0.140

layer indicating a growth of single phase domain during longer time anneal. The thickness of this film has increased by ~ 2 nm compared to the thickness after RTA [Fig. 2(b)] as a result of diffusion of the O_2 impurity in N_2 to the interface where oxidation of the substrate occurs.¹⁹ From Fig. 5(b), a ~ 3 -nm-thick layer of thermal SiO_2 has grown during the 600 s anneal. HfO_2 crystallites were observed in this film, again indicating that nucleation and growth occurred after SD during the annealing process. The DF image of this film was similar to Fig. 2(d). HfO_2 crystallites are not observed for films thinner than 12 nm even after anneal at 800 °C in N_2 for 600 s, which is not surprising since the onset of crystallization of HfO_2 in Hf silicate films depends on film composition²⁰ and thickness.²¹ In the nucleation and growth mechanism, for a nucleus to be stable to further growth, it must reach a critical size. Smaller nuclei are unstable and may dissolve because of surface energy effects and their large surface to volume ratio. Therefore the nucleation and growth process is suppressed in thinner films and a higher temperature is needed for crystallization to occur.²¹

It is difficult to resolve the layer closest to the (top) film surface from the glue that is used to prepare the TEM sample if that layer is Si rich. In order to examine the composition of this surface layer, ARXPS measurements were carried out and the results are presented in Table I for various photoelectron takeoff angles, θ . The Hf concentration, which is proportional to the Hf/(Hf+Si) ratio, decreases toward the surface for all films (which therefore implies an increase in the Si concentration). Comparing the Hf concentration in the as-grown and annealed films at $\theta=10^\circ$, more SiO_2 is observed to diffuse to the film surface during annealing, which suggests a wetting of the film surface by the SiO_2 -rich component. Previously, simulation results showed that the Si-rich phase contains >98 mol % SiO_2 in the $(\text{ZrO}_2)_x(\text{SiO}_2)_{1-x}$ system after phase separation during 900 °C anneals.⁸ Assuming that the Si-rich phase in the $(\text{HfO}_2)_{0.25}(\text{SiO}_2)_{0.75}$ films is pure SiO_2 , then the thickness of the surface layer of the films can be estimated. The escape depth (λ_e) of Si $2p$ photoelectrons excited by Al $K\alpha$ x rays in SiO_2 is 3 nm,¹⁸ which should be a reasonable estimate for Hf silicate films. The sampling depth then varies from 9 nm ($3\lambda_e$) at $\theta=90^\circ$ to 1.6

nm at $\theta=10^\circ$. Assuming that the film composition determined at $\theta=75^\circ$ corresponds to the average composition, then the thickness of the surface SiO_2 layer is estimated to be $\sim 0.4\text{--}0.7$ nm, i.e., equivalent to one to two layers of SiO_2 . The composition of the Hf-rich layer in the films shown in Fig. 1(b) or Fig. 2(b) can also be estimated from the relative thicknesses of the bright and dark layers. For example, the Hf-rich top and bottom layers evident in Fig. 2(b) have a composition $\text{Hf}/(\text{Hf}+\text{Si})\approx 0.32$. This value is much lower than the calculated composition ($\text{Zr}/(\text{Zr}+\text{Si})=0.80$) (Ref. 8) of the Zr-rich phase in the $\text{ZrO}_2\text{-SiO}_2$ system which experiences SD in this temperature range.

Using grazing-incidence small angle x-ray scattering (GISAXS), Stemmer *et al.*¹⁴ observed interference peaks in the horizontal cuts of their two-dimensional GISAXS intensity distribution, which correspond to a Hf concentration fluctuation in the plane of the film with λ_C values of 5 nm in the 4 nm $(\text{HfO}_2)_x(\text{SiO}_2)_{1-x}$ films ($x=0.4$) after 1000 °C annealing. The observation was confirmed by their plan-view TEM image, which shows interconnected Hf-rich and Si-rich regions. However, these authors did not try to interpret vertical cuts of their GISAXS data but still concluded that their observations were inconsistent with SDSD. In contrast, the TEM images reported here always show a layered structure for post-annealed films of thickness <8 nm, which is consistent with SDSD.

The diffusion coefficient of Hf in these $(\text{HfO}_2)_{0.25}(\text{SiO}_2)_{0.75}$ films can be estimated from our experimental observations. Based on the TEM images shown in Figs. 1(c) and 2(b), the diffusion length of Hf atoms after RTA should be ≥ 1 nm, which suggests a diffusion coefficient for Hf atoms in Hf silicate $\geq 10^{-19}$ m²/s at 800 °C.

In summary, the observation of SDSD in thin solid films is presented. While the configurations in as-grown and annealed $(\text{HfO}_2)_{0.25}(\text{SiO}_2)_{0.75}$ films are qualitatively in agree-

ment with the theory of SDSD, i.e., the composition waves normal to the film surface were observed, the observation that the composition of the film layer in contact with the substrate can be affected by film thickness has never been predicted by any SDSD simulation. Presumably, theoretical studies of SDSD could be modified to accommodate these experimental results. At this time, it is difficult to study SDSD in $(\text{HfO}_2)_{0.25}(\text{SiO}_2)_{0.75}$ films to determine whether the composition wave obeys the growth law $\lambda_C\sim t^{1/3}$ (Ref. 5) because: (i) TEM is a qualitative technique concerning atomic composition; (ii) SD in oxide systems is not easily controlled since the process occurs during the film deposition process; (iii) an alternative kinetic process, viz., nucleation and growth, can impede SD during the late stages of phase separation; and (iv) any O_2 impurity in the annealing N_2 ambient may also diffuse through the film and oxidize the substrate. While SDSD in the $(\text{HfO}_2)_{0.25}(\text{SiO}_2)_{0.75}$ thin films has been confirmed, the composition range for which $(\text{HfO}_2)_x(\text{SiO}_2)_{1-x}$ films experience SD and the resultant compositions of the phase-separated domains are still open questions.

The present observation of SDSD in $(\text{HfO}_2)_x(\text{SiO}_2)_{1-x}$ films may present significant device performance and reliability challenges for high- κ gate dielectric applications of pseudobinary alloy systems including $\text{ZrO}_2\text{-SiO}_2$, $\text{Y}_2\text{O}_3\text{-SiO}_2$, $\text{La}_2\text{O}_3\text{-SiO}_2$,⁸ etc., and have effects on thin film applications of any two-component system whose phase diagram shows a miscibility gap. The ALD growth mechanism for two-component films could also be influenced by SDSD if the film surface is preferentially attracted to one of the two components.

The authors are grateful for the technical assistance of L. Lebrun, G. Parent, and S. Moisa at NRCC and J. Hendriks at UWO. Financial assistance to W.N.L. was provided by NSERC (Canada).

¹J. W. Cahn, *Trans. Metall. Soc. AIME* **242**, 166 (1968).

²J. W. Cahn, *J. Chem. Phys.* **42**, 93 (1965).

³F. S. Bates and P. Wiltzius, *J. Chem. Phys.* **91**, 3258 (1989).

⁴R. A. L. Jones, L. J. Norton, E. J. Kramer, F. S. Bates, and P. Wiltzius, *Phys. Rev. Lett.* **66**, 1326 (1991).

⁵G. Krausch, C.-A. Dai, E. J. Kramer, and F. S. Bates, *Phys. Rev. Lett.* **71**, 3669 (1993).

⁶S. Puri and K. Binder, *Phys. Rev. E* **49**, 5359 (1994).

⁷S. K. Das, S. Puri, J. Horbach, and K. Binder, *Phys. Rev. E* **72**, 061603 (2005).

⁸H. Kim and P. C. McIntyre, *J. Appl. Phys.* **92**, 5094 (2002).

⁹P. A. Packan, *Science* **285**, 2079 (1999).

¹⁰J. Robertson, *Rep. Prog. Phys.* **69**, 327 (2006).

¹¹G. D. Wilk, R. M. Wallace, and J. M. Anthony, *J. Appl. Phys.* **87**, 484 (2000).

¹²M. A. Quevedo-Lopez, M. R. Visokay, J. J. Chambers, M. J. Bevan, A. LiFatou, L. Colombo, M. J. Kim, B. E. Gnade, and R. M. Wallace, *J. Appl. Phys.* **97**, 043508 (2005).

¹³D. A. Neumayer and E. Cartier, *J. Appl. Phys.* **90**, 1801 (2001).

¹⁴S. Stemmer, Y. Li, B. Foran, P. S. Lysaght, S. K. Streiffer, P. Fuoss, and S. Seifert, *Appl. Phys. Lett.* **83**, 3141 (2003).

¹⁵J. Liu, W. N. Lennard, L. V. Goncharova, D. Landheer, X. Wu, S. A. Ruchworth, and A. C. Jones, *J. Electrochem. Soc.* **156**, G89 (2009).

¹⁶T. Suntola, *Mater. Sci. Rep.* **4**, 261 (1989).

¹⁷J. Chen, W. J. Yoo, and D. S. H. Chan, *J. Electrochem. Soc.* **153**, G483 (2006).

¹⁸Z. H. Lu, J. P. McCaffrey, B. Brar, G. D. Wilk, R. M. Wallace, L. C. Feldman, and S. P. Tay, *Appl. Phys. Lett.* **71**, 2764 (1997).

¹⁹J.-P. Maria, D. Wicaksana, A. I. Kingon, B. Busch, H. Schulte, E. Garfunkel, and T. Gustafsson, *J. Appl. Phys.* **90**, 3476 (2001).

²⁰S. Stemmer, Z. Chen, C. G. Levi, P. S. Lysaght, B. Foran, J. A. Gisby, and J. R. Taylor, *Jpn. J. Appl. Phys., Part 1* **42**, 3593 (2003).

²¹G. Pant, A. Gnade, M. J. Kim, R. M. Wallace, B. E. Gnade, M. A. Quevedo-Lopez, and P. D. Kirsch, *Appl. Phys. Lett.* **88**, 032901 (2006).